State preparation and detector effects in quantum measurements of rotation with circular polarization-entangled photons and photon counting

Longzhu Cen, Zijing Zhang,* Jiandong Zhang, Shuo Li, Yifei Sun, Linyu Yan, and Yuan Zhao†
Department of Physics, Harbin Institute of Technology, Harbin 150001, China

Feng Wang
Tianjin Jinhang Institute of Technological Physics, Tianjin 300192, China
(Received 28 April 2017; published 21 November 2017)

Circular polarization-entangled photons can be used to obtain an enhancement of the precision in a rotation measurement. In this paper, the method of entanglement transformation is used to produce NOON states in circular polarization from a readily generated linear polarization-entangled photon source. Detection of N-fold coincidences serves as the postselection and N-fold superoscillating fringes are obtained simultaneously. A parity strategy and conditional probabilistic statistics contribute to a better fringe, saturating the angle sensitivity to the Heisenberg limit. The impact of imperfect state preparation and detection is discussed both separately and jointly. For the separated case, the influence of each system imperfection is pronounced. For the joint case, the feasibility region for surpassing the standard quantum limit is given. Our work pushes the state preparation of circular polarization-entangled photons to the same level as that in the case of linear polarization. It is also confirmed that entanglement can be transformed into different frames for specific applications, serving as a useful scheme for using entangled sources.

DOI: 10.1103/PhysRevA.96.053846

I. INTRODUCTION

Recent developments in quantum metrology have obtained a superior performance for estimation precision that surpasses the standard quantum limit (SQL) that bounds the classical method [1], with the prominent example of entangled multiphoton states improving interferometric techniques. Many of these studies have investigated the so-called NOON states,

$$|N::0\rangle_{A,B} = \frac{1}{\sqrt{2}}(|N,0\rangle_{A,B} + |0,N\rangle_{A,B}), \tag{1}$$

which possess maximal path-entanglement between paths A and B. In optics and more specifically in the frame of linear polarization, a NOON state can be an equal superposition of states that combine all N photons in either horizontal (H) or vertical (V) polarization mode, denoted as $|N::0\rangle_{H,V}$. By utilizing this kind of NOON state in a conventional interferometer; for example, a Mach–Zehnder type, one can acquire a phase N times faster than for classical light [2]. This implies that the phase sensitivity is enhanced to surpass the SQL and reaches the more fundamental Heisenberg limit [3], and the phase resolution is enhanced to realize sub-Rayleigh-resolution quantum lithography [4].

Although linearly polarized photons are not inherently required to form a NOON state, the linear polarization frame is used in most experiments because the linear polarizer can be easily obtained and the phase estimation is of greater interest [5–10]. However, it has been noted that a NOON state in the frame of circular polarization, denoted as $|N::0\rangle_{L,R}$ where L and R represent left- or right-circular polarization modes, respectively, can be used to achieve a quantum-enhanced rotation measurement similar to the phase measurement [11]. Additionally, experimental research has been reported for the probing of a delicate material system by means of near-resonant Faraday rotation where the $|N::0\rangle_{L,R}$ states enable a quantum enhancement [12]. Unfortunately, the number of photons involved in a single detection is limited to two, much less than what has been realized in the linear polarization frame [5]. Given that the use of NOON states becomes increasingly advantageous with increasing number of photons, a practical scheme of rotation measurement in which $|N::0\rangle_{L,R}$ with a larger N is utilized seems appealing and feasible.

The concept of entanglement transformation has been widely exploited to produce entanglement in different degrees of freedom from parametric downconversion photon pairs [13,14]. From our perspective, entanglement transformation from linear polarization frame to the circular polarization frame is expected. In this paper, we point out that one can easily make the frame transformation of NOON states from $|N::0\rangle_{H,V}$ to $|N::0\rangle_{L,R}$ by a properly placed quarter-wave plate. Since the states of $|N::0\rangle_{H,V}$ have been experimentally generated up to $N = 5$ [5], we follow their result in our rotation measurement scheme to produce $|N::0\rangle_{L,R}$ of the same size. Photon counting is implemented in the measurement stage to obtain N-fold coincidence, which plays a key role in achieving super-resolution and supersensitivity. Most importantly, the influence of source and detector imperfections on the estimate performance is discussed in detail and the threshold for obtaining better performance than that of the classical method is given.

II. THE SCHEME: QUANTUM MEASUREMENT OF ROTATION

The measurement setup of rotation is shown in Fig. 1. In the following section, this kind of measurement scheme will be discussed in the three stages shown in Fig. 1.

*zhangzijing@hit.edu.cn
†zhaoyuan@hit.edu.cn

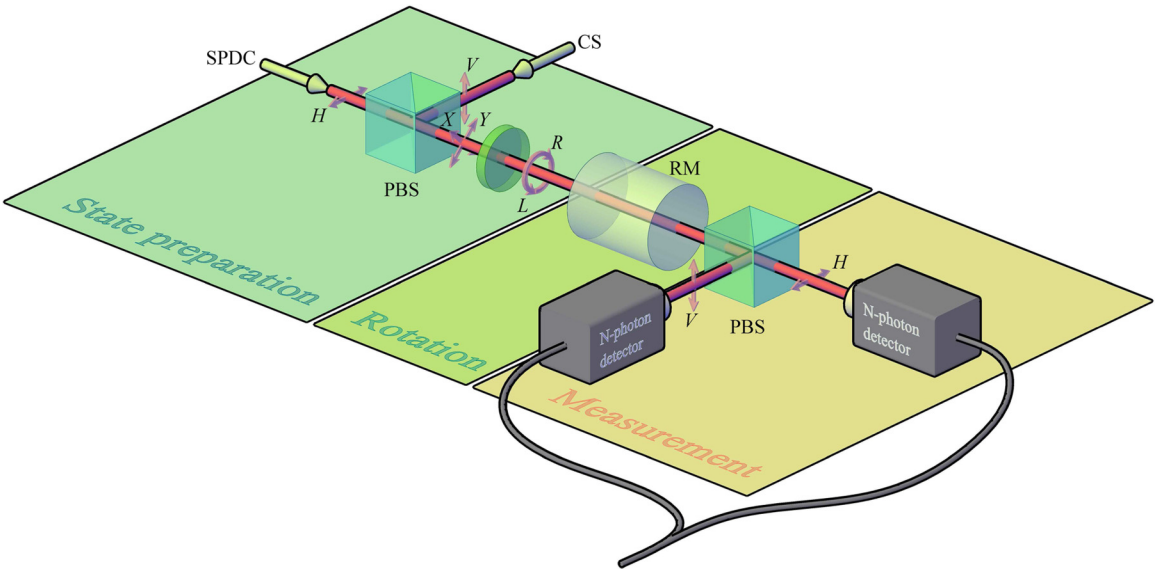

FIG. 1. Illustration of quantum rotation measurement. The first polarizing beam splitter (PBS) that reflects horizontal polarized photons and transmits vertical polarized photons is fed by coherent light (CS) and spontaneous parametric down-converted light (SPDC) in its two input ports in polarizations H and V. The generated state, polarized at angle $\pm 45^\circ$ to the horizontal plane (X and Y polarizations), is transformed by a QWP into the frame of circular polarization and is rotated by a rotation medium (RM). The photons are then projected onto horizontal or vertical polarization states at the second PBS and two photon-number-resolving apparatuses on each polarization output record all the possible outcomes.

A. State-preparation stage

In the stage of state preparation, the state $|N::0\rangle_{L,R}$ is produced by entanglement transformation from linear to circular polarization. To analysis this process, we first expand $|N::0\rangle_{L,R}$ onto a two-mode Fock basis of linear polarization as (see Appendix A for derivation in detail)

$$|N::0\rangle_{L,R} = \mathcal{C}_N \sum_{k=0}^{N} \binom{N}{k}^{1/2} [i^k + i^{N-k}] |k\rangle_H |N-k\rangle_V . \tag{2}$$

where $\mathcal{C}_N = (1/\sqrt{2})^{N+1}$. With $|N::0\rangle_{H,V}$ and $|N::0\rangle_{R,L}$ expressed in the same basis, we can now investigate the entanglement transformation. It is well known in classical optics that a circularly polarized light can be obtained by placing a quarter-wave plate behind a linearly polarized light. We confirm that this process still holds for photons in Fock states. Consider an input state of $|N::0\rangle_{H,V}$ to be transformed by a quarter-wave plate for which the fast axis is rotated away from the H direction by angle β; then, the unitary transformation associated with the impact on the input state can be expressed as [15,16]

$$\hat{U}_{\mathrm{QWP}}(\beta) = e^{i2\beta \hat{J}_y} e^{i(\pi/2)\hat{J}_z} e^{-i2\beta \hat{J}_y} . \tag{3}$$

The fidelity of the output state $|\psi_{\mathrm{out}}\rangle$ with $|N::0\rangle_{L,R}$ is $F_N \equiv |_{L,R}\langle N::0 \mid \psi_{\mathrm{out}}\rangle|^2$. By simple calculation, we obtained that F_N saturates to unity when $\beta = 45^\circ$, implying the perfect transformation from $|N::0\rangle_{H,V}$ to $|N::0\rangle_{R,L}$. Finally, in our scheme, the readily generated linearly polarized NOON overlap is transformed into circular polarization-entangled photons as is shown in Fig. 2. The corner-like shape in Fig. 2(c) illustrates the tendency of all photons to collectively stay in the same mode.

B. Rotation stage

The produced state propagates to accumulate a rotation of the optical polarization with an angle of θ, in a rotation

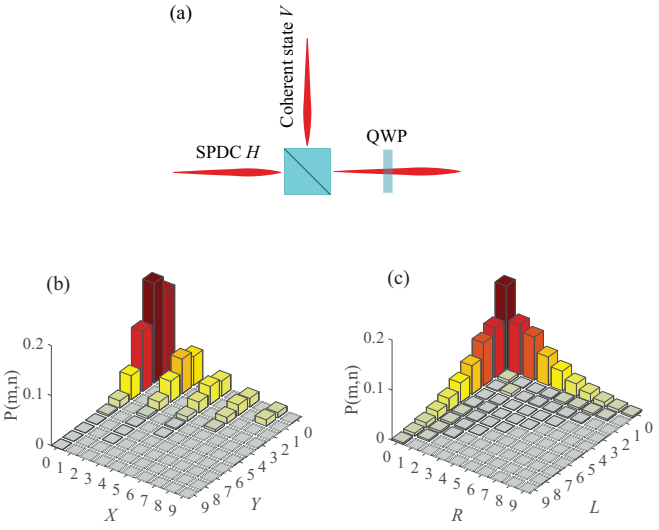

FIG. 2. Scheme of state preparation and theoretical properties of the generated states. (a) NOON states in the frame of linear polarization are produced by mixing H polarized collinear degenerate spontaneous parametric down-conversion (SPDC) and a V polarized coherent state at a polarizing beam splitter and are further transformed into the circular polarization frame by a quarter-wave plate (QWP). (b) $|N::0\rangle_{R,L}$ overlap in the linear polarization basis. X and Y contribute $\pm 45^\circ$ polarization, respectively. Bar heights represent the probability for m, n photons in polarization modes X, Y, respectively. (c) The same as panel (b) but in the circular polarization basis.

medium (RM) in the rotation stage. The effect of RM can be realized by a DOVE prism [17], or by a magneto-optic material that induces a resonantly enhanced Faraday rotation with respect to the applied axial magnetic field B [12], or simply by setting a relative angle between the reference frames of state-preparation and measurement setup [11]. The rotation is encoded onto each of the NOON states, resulting in

$$|\psi_N\rangle = \frac{1}{\sqrt{2}}(e^{iN\theta}|N,0\rangle_{R,L} + e^{-iN\theta}|0,N\rangle_{R,L}). \tag{4}$$

The coherent superposition of $e^{iN\theta}|N,0\rangle_{L,R}$ and $e^{-iN\theta}|0,N\rangle_{L,R}$ lies at the heart of the entanglement. To ensure the feasibility of our scheme, it must be verified first and actually has been experimentally demonstrated by Afek *et al.* [5]. In their scheme for phase measurement, similar superpositions expressed by Eq. (4), which leads to the observation of superresolution and supersensitivity. This is the general method to take advantage of entangled sources and is also implemented in our scheme.

C. Measurement stage

After leaving the rotation stage, the photons are projected onto horizontal or vertical polarization states at the second PBS, and coincidences of different combination are recorded by two N-photon detectors. The probability for detecting exactly m photons in H and $N-m$ photons in V is

$$P_{m,N-m}(\theta) = |_{H,V}\langle m,N-m|\psi_N\rangle|^2 \tag{5}$$

for $m = 0,\ldots,N$. These probabilities are known to exhibit superoscillations [11,12], and thus can increase the angle sensitivity. The uncertainty of estimating θ by $P_{m,N-m}$ is

$$\Delta\theta_{m,N-m} = \frac{\Delta P_{m,N-m}}{\left|\frac{\partial P_{m,N-m}}{\partial\theta}\right|}, \tag{6}$$

where the uncertainty associated with $P_{m,N-m}$ is $\Delta P_{m,N-m} = (P_{m,N-m} - P^2_{m,N-m})^{1/2}$ [3,18,19]. This uncertainty is bounded by the Heisenberg limit of the rotation measurement, $\Delta\theta_{m,N-m} \geqslant 1/2N$, which is different from that of the phase measurement by a constant factor of two [11].

To illustrate the detection performance of such a setup, we take the condition of a pure $|5::0\rangle_{R,L}$ state and perfect photon-number-resolving detectors, for example. The results are shown in Fig. 3. The probability of three photons in H polarization and two photons in V polarization is calculated and shows a de Broglie wavelength [2] of $\lambda/5$, as expected. Notably, the peak value of $P_{3,2}$ does not reach unity because of the missing recorded events other than 3, 2 and 2, 3, and for the same reason the sensitivity approaches the Heisenberg limit (shown by the shaded area) but does not actually reach it. With the peak value of a, the minimum sensitivity is $1/[2N\sqrt{a}]$. The lack of saturation for the Heisenberg limit can be addressed. There are two basic data processing methods. The first is quite similar to the strategy of parity measurements [20,21]. Considering that the coincidence fringes of $P_{m,N-m}$ for any even or odd m are in-phase, the superposition of all the $P_{2k,N-2k}$ or $P_{2k+1,N-2k-1}$ must be constructive. As for the pure $|N::0\rangle_{L,R}$ input, it can be demonstrated that the peak value of $\sum_{k=0}^{[N/2]} P_{2k,N-2k}$ or $\sum_{k=0}^{[N/2]} P_{2k+1,N-2k-1}$ will saturate

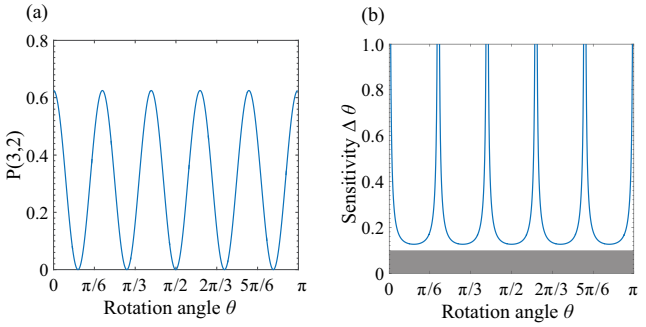

FIG. 3. Theoretical result of rotation measurement on the condition of using pure $|5::0\rangle_{R,L}$ state and perfect photon-number-resolving detectors. (a) Simulated fivefold coincidences as a function of rotation angle. $P_{3,2}$ oscillates five times faster than predicted by the Malus law, showing fivefold super-resolution. (b) Theory of angle sensitivity. The Heisenberg limit, shaded area, is not reached because of the inadequate utilization of all outcome events.

to unity and the therefore the Heisenberg limit is reached. For the case with noise, even we take an even or odd superposition of the coincidence fringes, the peak value will not saturate to unity because the noise with higher or lower photons does not contribute to coincidence. In this situation, another data processing method of measuring the conditional probability should be considered [7]. In this method, $\sum_k^{[N/2]} P_{2k,N-2k}$ or $\sum_{k=0}^{[N/2]} P_{2k+1,N-2k-1}$ is normalized by the probability of total coincidence $P_N = \sum_{k=0}^{N} P_{k,N-k}$ to obtain the conditional probability as

$$\widetilde{P}_{\rm odd}(\theta) = \frac{1}{P_N}\sum_{k=0}^{[N/2]} P_{2k,N-2k},$$
$$\widetilde{P}_{\rm even}(\theta) = \frac{1}{P_N}\sum_{k=0}^{[N/2]} P_{2k+1,N-2k-1}. \tag{7}$$

It will be shown that either $\widetilde{P}_{\rm odd}(\theta)$ or $\widetilde{P}_{\rm even}(\theta)$ can be used to saturate the angle sensitivity as close as possible to the Heisenberg limit.

III. IMPACT OF SYSTEM IMPERFECTIONS

Due to the NOON-state-preparation method and experiment limitations, the actual measurement result will deviate from the ideal situation shown in Fig. 3. As discussed in Ref. [22], the influence of the experimental limitations mainly arises from imperfect states and detectors. Here, we first take into account each of these aspects separately and then proceed to the combined effect.

A. Imperfect state preparation

The state used here for rotation measurement is an overlap of $|N::0\rangle_{R,L}$ for arbitrary N. For each N-photon component, the fidelity with $|N::0\rangle_{R,L}$ does not saturate to unity completely. After we record the coincident rate of m photons in H polarization and $N-m$ photons in V polarization, a postselection of the N-photon component is actually performed, and

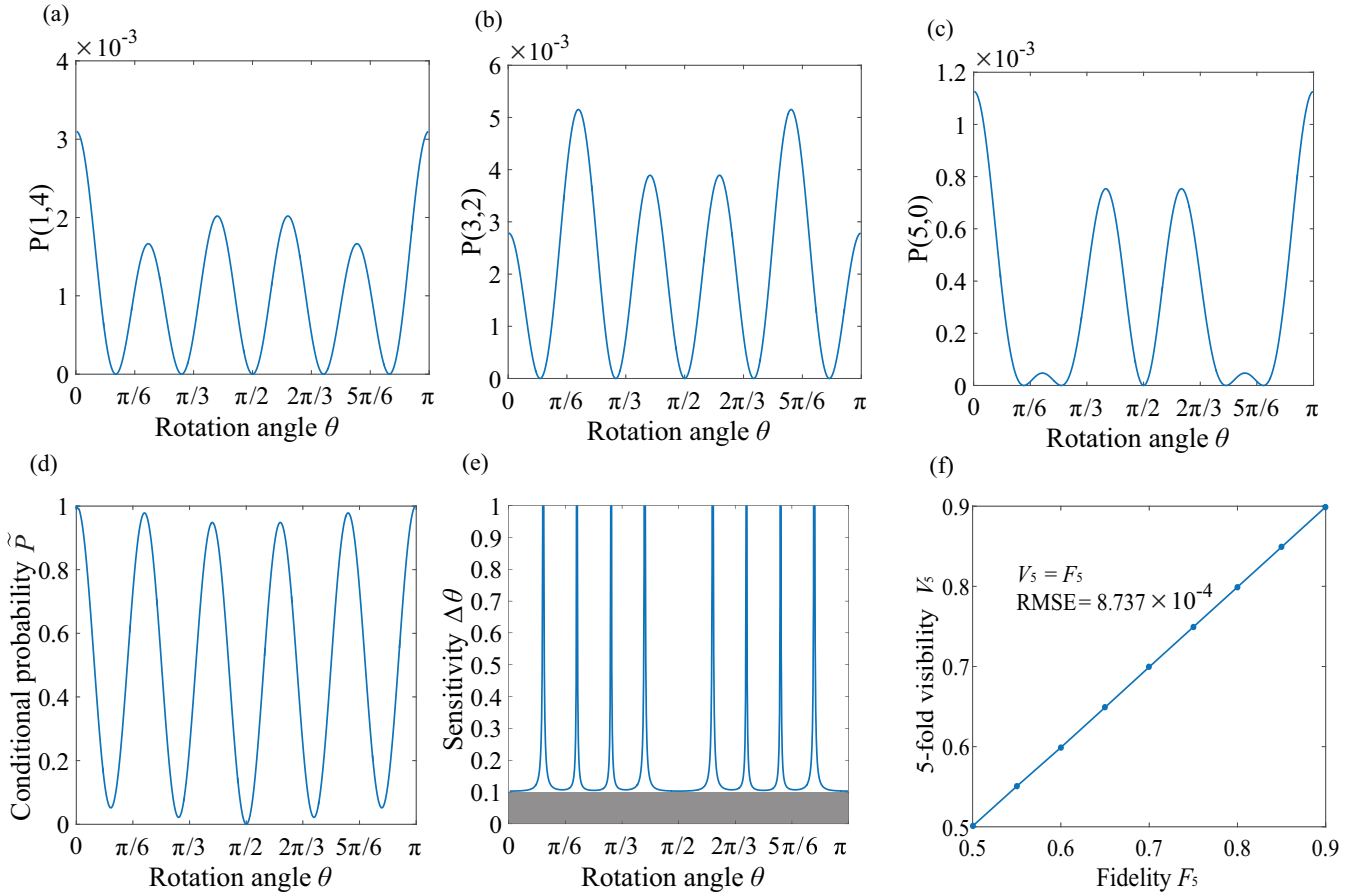

FIG. 4. Theoretical result of rotation measurement on the condition of practical source and perfect photon-number-resolving detectors. (a)–(c) Coincident rate of events in which the number of photons of H polarization is odd. (d) Conditional probability obtained by superimposing fringes in panels (a)–(c) and normalized by the proportion of a five-photon component in the overlap c. (e) Angle sensitivity associated with the conditional probability of panel (d), Heisenberg limit, shaded area, is saturated at certain angle. (f) Fivefold visibility of conditional probability vs the fidelity of five-photon components. The data points are fit by $V_5 = F_5$ with a root-mean-square error (RMSE) of 8.737×10^{-4}.

the other component serves as noise and eventually reduces the peak value of $P_{m,N-m}$, which is harmful for the sensitivity, as discussed above. Taking c as the proportion of the N-photon component in the overlap, it is obvious that $c = P_N$ and serves as the normalization coefficient in the process of obtaining the conditional probability as expressed in Eq. (7).

Except for the noise from the "non-N" components, there exist "non-NOON" components among the N-photon components that may affect the coincident signal rate. More specifically, the fidelity of N-photon components with $|N :: 0\rangle_{R,L}$ controls the visibility of the N-fold oscillations [23]. To study the visibility of coincidence fringes, we consider an arbitrary $P_{m,N-m}$ in the form of a Fourier series:

$$P_{m,N-m}(\theta) = \sum_{k=0}^{\infty} A_k \cos(2k\theta + \delta_k). \tag{8}$$

$|A_N/A_0|$ is referred to as the N-fold visibility V_N. For pure sinusoidal oscillations with a constant background, the N-fold visibility coincides with the conventional definition of visibility. In our case, the actual probability for detecting m photons in H polarization and $N-m$ photons in V polarization is given by

$$P_{m,N-m}(\theta) = \mathrm{Tr}[\hat{U}_{GR}(\theta)|\psi\rangle\langle\psi|\hat{U}_{GR}^{\dagger}(\theta)|m\rangle\langle m|_H \otimes |N-m\rangle\langle N-m|_V], \tag{9}$$

where $\hat{U}_{GR}(\theta) = e^{i2\theta\hat{J}_y}$ is a unitary operator describing the rotation using the angular-momentum notation [15]. $|\psi\rangle$ is the $|N :: 0\rangle_{R,L}$ overlap obtained in the state-preparation stage. The result is shown in Fig. 4. Fringes of $P_{1,4}$, $P_{3,2}$, $P_{5,0}$ can hardly possess a fivefold visibility of unity. However, a superposition of these three fringes will lead to an improved result, as shown in Fig. 4(d) where normalization has been already performed. Using this fringe, the Heisenberg limit is saturated at a certain angle. The fringe of Fig. 4(d) shows nearly perfect fivefold super-resolution and the imperfection is due to imperfect fidelity. We fit the experimental curves to a Fourier series of the form expressed in Eq. (8) and truncated at $k = 5$ and find that N-fold visibility is exactly equal to the fidelity of the input state, as shown in Fig. 4(f). This is quite understandable because "non-NOON" components are orthotropic to the NOON state and will never contribute to an N-fold fringe.

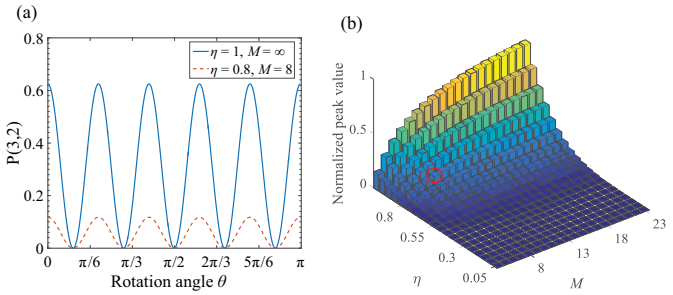

FIG. 5. Effect of approximate photon-number-resolving detection on the condition of using the pure $|5::0\rangle_{R,L}$ state. (a) Comparison of the detected results of $P_{3,2}$ between perfect and approximate photon-number-resolving detector. For the approximate detector, the overall transmission $\eta = 0.8$ and number of bins involved in time-multiplexed process, $M = 8$, are given. The perfect case can be regarded as $\eta = 1$ and $M = \infty$. (b) Peak values of approximately detected $P_{3,2}$ against M and η, normalized by that of the perfect case, 0.625. Red circle indicates the situation of panel (a).

B. Imperfect detection

The original proposal of recording the coincident rate assumed completely-photon-number-resolving detectors that implement projections onto all Fock states, which is far behind the state of the art achievable by using current techniques and experimental conditions [24]. Therefore, an approximate photon-number-resolving detection using a multiplexed method is proposed [5,7,9,25]. This scheme takes advantage of readily available components such as avalanche photodiodes and time-multiplexed devices [26]. In this scheme, the incoming pulse is split into many spatially or temporally separate bins, making the presence of more than one photon per bin unlikely. Subsequently, all bins are detected with two APDs. Photon-number resolution is then obtained by summing the number of one-click outcomes from all of the bins.

This kind of photon-number-resolving detector is well characterized by the positive-operator-value-measure (POVM) formalism [27,28] in which all photon-counting operations correspond to the POVM elements $\hat{\pi}_n$:

$$\hat{\pi}_n = \sum_{k=0}^{\infty} \theta_{n,k} |k\rangle\langle k|, \quad \theta_{n,k} = [C_M L(\eta)]_{n,k}, \tag{10}$$

where n, k, and M denote the detection pattern, the photon number, and the number of bins involved in the time-multiplexed process, respectively. The POVM introduces experimental imperfections via two matrices, C_M and L_η, which characterize weights and loss (see Appendix B for explicit dependence).

We now elucidate the performance of such a photon-number-resolving detector and its drawbacks compared with the ideal case. We consider an input state of pure $|5::0\rangle_{R,L}$ and rewrite Eq. (9) to obtain the detecting signal as

$$P_{m,N-m}(\theta) = \mathrm{Tr}[\hat{U}_{GR}(\theta)|5::0\rangle_{R,L}\langle 5::0|\hat{U}^{\dagger}_{GR}(\theta)\hat{\pi}^{H}_{m} \otimes \hat{\pi}^{V}_{N-m}]. \tag{11}$$

Figure 5(a) shows the detecting result under such conditions. We find surprisingly that the fringes of $P_{3,2}$ are quite similar to the theoretical prediction for the ideal case of Fig. 3(a). The only difference is that the peak value shifts further away from unity and can be solved by measuring the conditional probability. Figure 5(b) shows the peak value of $P_{3,2}$, normalized by the peak value of the ideal case $a = 0.625$, varying with M and η. The normalized peak value of $P_{3,2}$ is mainly controlled by η as it decreases sharply with the decrease of η. Increasing M does enhance the normalized peak value but the effect becomes inconspicuous for large M and the enhancement is quickly degraded by a low η. For the actual available components and optical arrangement, η can be barely higher than 0.5 [5,6,28]; in this case there is no need to arrange redundant bins in the photon-number-resolving detectors.

It is notable that, on the one hand, the approximate photon-number-resolving detector does not damage the visibility of coincidence fringes on the condition of pure $|N::0\rangle_{R,L}$ input. On the other hand, this does not mean that this effect is also obtained for the noisy input conditions. Considering the detecting principle of this kind of detectors, it is easy to show that, for the POVM element of $\hat{\pi}_n$, the noisy input states for which the photon numbers $N < n$, called low-photon noise, will admit no influence on the measuring result (dark count is omitted). In contrast, the states for which the photon numbers $N > n$, called the high-photon noise, affect the detection outcomes. This effect is absent on the condition of pure $|N::0\rangle_{R,L}$ input and we discuss it in the next section.

C. Imperfect state preparation and detection

Finally, we take the imperfect state preparation and detection into account together and discuss their combined effect. The effects of high photon noise and approximate photon-number-resolving detection will both be magnified. In this situation, Eq. (9) is rewritten to obtain the detecting signal as

$$P_{m,N-m}(\theta) = \mathrm{Tr}\big[\hat{U}_{GR}(\theta)|\psi\rangle\langle\psi|\hat{U}^{\dagger}_{GR}(\theta)\hat{\pi}^{H}_{m} \otimes \hat{\pi}^{V}_{N-m}\big]. \tag{12}$$

Taking $N = 5$ as an example, the obtained results are plotted in Fig. 6. Due to the detecting principle of the approximate photon-number-resolving detector, a coincident outcome of $m, 5-m$ event may result from high-photon noise and, consequently, the possibility of outcomes with a sum number of five, P_5, is no longer constant. Rather, this probability varies with respect to the rotation angle as shown in the plot of Fig. 6(a). Therefore, the conditional probability of detecting events with even m becomes

$$\widetilde{P}_{\mathrm{even}}(\theta) = \frac{1}{P_5(\theta)} \sum_{k=0}^{2} P_{2k+1,5-2k-1}. \tag{13}$$

The fringe is plotted in Fig. 6(b) and shows an obvious visibility decline compared with the fringe in Fig. 4(d). The fivefold visibility equals 75.06% and the sensitivity does not saturate to the Heisenberg limit but is still lower than the SQL. All of the results presented in Figs. 6(a)–6(c) are obtained under conditions in which the detector parameters are $M = 15$, $\eta = 1$ and the fidelity of five-photon components with $|5::0\rangle_{R,L}$ is 0.94. This is a quite ideal conditions, especially for $\eta = 1$. The effect of increasing M has become

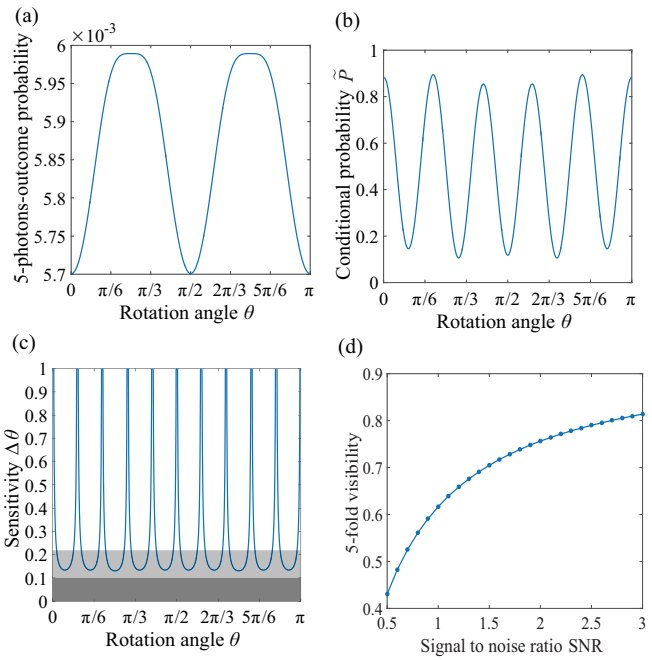

FIG. 6. Theoretical result of rotation measurement on the condition of practical source and photon-number-resolving detectors. (a) Probability of outcomes with a sum photon-number of five. (b) Conditional probability of the N-fold coincident events signal. (c) Angle sensitivity associated with the conditional probability of panel (b). The light and deep shaded areas indicate the SQL and the Heisenberg limit, respectively. (d) Fivefold visibility of conditional probability vs the SNR of the source.

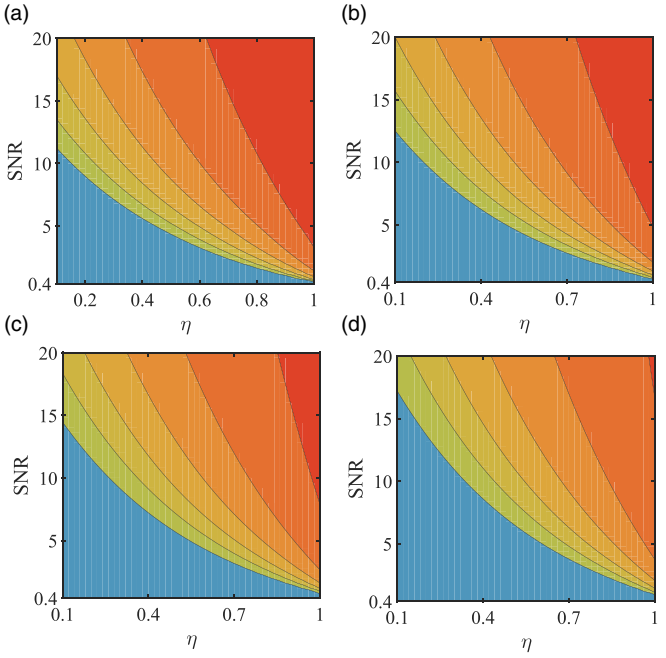

FIG. 7. Minimum sensitivity as a function of the overall transmission η and of the signal-to-noise ratio (SNR) for different values of the fidelity of five-photon components F_5: (a) $F_5 = 0.94$, (b) $F_5 = 0.84$, (c) $F_5 = 0.74$, (d) $F_5 = 0.64$. Darker regions correspond to higher sensitivity. The values of contour lines from left to right in each plot are 0.22 (SQL), 0.20, 0.18, 0.16, 0.14, and 0.12. The Heisenberg limit (0.1) is not reached.

unimportant. In this case, the high-photon noise becomes the only problematic effect that is responsible for the degradation of the detecting performance; as shown in Fig. 6(d), in this case, with the increase of signal to noise ratio (SNR), the fivefold visibility increases and approaches the upper limit, which is exactly equal to the fidelity of five-photon components with $|5 :: 0\rangle_{R,L}$.

The quantum advantage of $|N :: 0\rangle_{L,R}$ is addressed by (F_N, SNR, η, M). To advance toward quantum-enhanced rotation measurements, it is important to determine the experimental conditions required to surpass the SQL. We find numerically that (F_N, SNR, η) have the strongest effect on the sensitivity, while M is a minor factor that is merely required to be greater than N. For $N = 5$, the contour plot of minimum sensitivity reached for certain combinations of (F_N, SNR, η) is shown in Fig. 7 where a slight difference can be obtained by changing M. In general, lower η requires higher SNR to reach the same minimum sensitivity. As F_N decreases, the quantum region, bounded by the leftmost contour line, decreases, and the feasibility region shrinks more sharply as for the sensitivity of higher level. To the best of our knowledge, currently there is no efficient method to increase the SNR in the photon number level. In fact, the coincident record serves as a general method of postselection and can filter noise but is unfortunately limited by the practical photon-number-resolving detector. This makes the increase of even more significant η. To reach an even higher sensitivity than that of the SQL, the fidelity of the produced state with $|N :: 0\rangle_{R,L}$ is also crucial.

IV. CONCLUSIONS

We have demonstrated a practical quantum rotation measurement scheme from the state-preparation stage to the measurement stage. In the state-preparation stage, the method of entanglement transformation is used to produce NOON states in circular polarization from a readily generated linear polarization-entangled photon source. In the measurement stage, the coincident rate is recorded and even or odd superposition is taken onto the obtained fringes. Both superresolution and supersensitivity can be reached. Most importantly, we have identified the major imperfections in the experiment: the fidelity and SNR of the input state, the overall transmission, and the time-multiplexed bin number of practical photon-number-resolving detectors. We have shown that the first three of these are the most detrimental to the sensitivity and conclude that the joint analysis of these three factors may help reach a different level of estimation performance by using equipment advantageous for different factors.

In addition, even though it was found that a considerable quantum region remains in the parameter space considered in this work, NOON states are notoriously sensitive to photon loss. Other quantum states such as Gaussian [29] and optimal states [30] can be used instead. In fact, our work is also originally based on Gaussian states. The setup shown in Fig. 2(a) mixing a coherent state and a squeezed vacuum state at a beam splitter is a quite classical arrangement that has been widely investigated. Schemes based on this kind of setup for phase measurement have been reported [31,32]. We find that these schemes show different characteristics and

satisfy different requirements. The main difference among these schemes, including ours, is the data processing method. That is, one can easily switch between these methods without changing the arrangement of any optical or electrical elements for the implementation of the experiments. The setups will be effective for the needs of a particular case but not for the typical method.

APPENDIX A: EXPANSION OF $|N :: 0\rangle_{L,R}$ ONTO TWO-MODE FOCK BASIS OF LINEAR POLARIZATION

We begin the derivation of representation conversion by defining the annihilation operator of an L- or R-polarized photon as $\hat{a}_L$ or $\hat{a}_R$. These operators and their Hermitian conjugates satisfy the boson commutation relations:

$$[\hat{a}_i,\hat{a}_j]=[\hat{a}_i^\dagger,\hat{a}_j^\dagger]=0,\quad [\hat{a}_i,\hat{a}_j^\dagger]=\delta_{ij}, \tag{A1}$$

where i and j take on the values L and R. Given that a single-photon state of linear polarization or circular polarization satisfies the relations

$$\begin{aligned}|1\rangle_R &= \frac{1}{\sqrt{2}}(|1\rangle_H+i|1\rangle_V)=\frac{1}{\sqrt{2}}(\hat{a}_H^\dagger+i\hat{a}_V^\dagger)|0\rangle,\\ |1\rangle_L &= \frac{1}{\sqrt{2}}(i|1\rangle_H+|1\rangle_V)=\frac{1}{\sqrt{2}}(i\hat{a}_H^\dagger+\hat{a}_V^\dagger)|0\rangle,\end{aligned} \tag{A2}$$

one may conclude that $(\hat{a}_H^\dagger+i\hat{a}_V^\dagger)/2$ and $(i\hat{a}_H^\dagger+\hat{a}_V^\dagger)/2$ is the creation operator of an L or R polarized photon. Namely,

$$\begin{pmatrix}\hat{a}_R^\dagger\\ \hat{a}_L^\dagger\end{pmatrix}=\frac{1}{\sqrt{2}}\begin{pmatrix}1 & i\\ i & 1\end{pmatrix}\begin{pmatrix}\hat{a}_H^\dagger\\ \hat{a}_V^\dagger\end{pmatrix}. \tag{A3}$$

This can be further confirmed by comparing with the well-known rotation operator [15]

$$\hat{J}_y=-\frac{i}{2}(\hat{a}_H^\dagger\hat{a}_V-\hat{a}_H\hat{a}_V^\dagger). \tag{A4}$$

Since the L and R polarization states are eigenstates of rotation, $\hat{J}_y$ can also be expressed as

$$\hat{J}_y=\tfrac{1}{2}(\hat{a}_R^\dagger\hat{a}_R-\hat{a}_L^\dagger\hat{a}_L). \tag{A5}$$

By substituting Eq. (A3) into Eq. (A5), one can easily obtain Eq. (A4), which is certainly the verification of Eq. (A3).

With the relation of Eq. (A3), we can now expand $|N :: 0\rangle_{L,R}$ onto the two-mode Fock linear polarization basis:

$$|N :: 0\rangle_{L,R}=\mathcal{C}_N\sum_{k=0}^{N}\binom{N}{k}^{1/2}[i^k+i^{N-k}]|k\rangle_H|N-k\rangle_V, \tag{A6}$$

where $\mathcal{C}_N=(1/\sqrt{2})^{N+1}$.

APPENDIX B: EXPLICIT DEPENDENCE OF DETECTOR CHARACTERIZER ON EXPERIMENTAL IMPERFECTIONS

L_η characterize loss and $[L_\eta]_{m,k}$ is the conditional probability that $k-m$ photons are loss when $k-1$ photons are incident. By using the abstract loss model [25], the loss of the sources can be accounted by a single parameter η representing the overall transmission. The nonzero loss matrix elements are given by

$$[L_\eta]_{m,k}=\binom{k-1}{m-1}\eta^{m-1}(1-\eta)^{k-m},\quad m,k=1,2,\ldots. \tag{B1}$$

C_M characterize the weights and, for an approximate photon-number-resolving detector that contains M bins in a time-multiplexed setup, $[C_M]_{n,m}$ is the conditional probability that $n-1$ counts are detected when $m-1$ photons are retained from the loss. The calculation of the conditional probabilities can be reduced to a simple stochastic model of distributing $m-1$ balls into M baskets and calculating the probability that $n-1$ baskets are occupied. Let $X_{n,m}$ be the number of the patterns for which m balls occupy n baskets, which satisfy the recursion relation of

$$X_{n,m}=n^m-\sum_{i=1}^{n-1}\binom{n}{i}X_{i,m}. \tag{B2}$$

Then, $[C_M]_{n,m}$ can be calculated by

$$[C_M]_{n,m}=\binom{M}{n-1}X_{n-1,m-1}/M^{m-1}. \tag{B3}$$

[1] V. Giovannetti, S. Lloyd, and L. Maccone, Science **306**, 1330 (2004).

[2] C. Gerry and P. Knight, *Introductory Quantum Optics* (Cambridge University Press, 2005).

[3] J. P. Dowling, Contemp. Phys. **49**, 125 (2008).

[4] A. N. Boto, P. Kok, D. S. Abrams, S. L. Braunstein, C. P. Williams, and J. P. Dowling, Phys. Rev. Lett. **85**, 2733 (2000).

[5] I. Afek, O. Ambar, and Y. Silberberg, Science **328**, 879 (2010).

[6] J. C. Matthews, X.-Q. Zhou, H. Cable, P. J. Shadbolt, D. J. Saunders, G. A. Durkin, G. J. Pryde, and J. L. O'Brien, npj Quantum Inf. **2**, 16023 (2016).

[7] Y. Israel, S. Rosen, and Y. Silberberg, Phys. Rev. Lett. **112**, 103604 (2014).

[8] H. Cable and G. A. Durkin, Phys. Rev. Lett. **105**, 013603 (2010).

[9] G.-Y. Xiang, B. L. Higgins, D. Berry, H. M. Wiseman, and G. Pryde, Nat. Photonics **5**, 43 (2011).

[10] M. W. Mitchell, J. S. Lundeen, and A. M. Steinberg, Nature (London) **429**, 161 (2004).

[11] V. D'ambrosio, N. Spagnolo, L. Del Re, S. Slussarenko, Y. Li, L. C. Kwek, L. Marrucci, S. P. Walborn, L. Aolita, and F. Sciarrino, Nat. Commun. **4**, 2432 (2013).

[12] F. Wolfgramm, C. Vitelli, F. A. Beduini, N. Godbout, and M. W. Mitchell, Nat. Photonics **7**, 28 (2013).

[13] R. Fickler, R. Lapkiewicz, W. N. Plick, M. Krenn, C. Schaeff, S. Ramelow, and A. Zeilinger, Science **338**, 640 (2012).

[14] E. Nagali, F. Sciarrino, F. De Martini, L. Marrucci, B. Piccirillo, E. Karimi, and E. Santamato, Phys. Rev. Lett. **103**, 013601 (2009).

[15] B. Yurke, S. L. McCall, and J. R. Klauder, Phys. Rev. A **33**, 4033 (1986).
[16] P. Usachev, J. Söderholm, G. Björk, and A. Trifonov, Opt. Commun. **193**, 161 (2001).
[17] O. S. Magaña-Loaiza, M. Mirhosseini, B. Rodenburg, and R. W. Boyd, Phys. Rev. Lett. **112**, 200401 (2014).
[18] G. Khoury, H. S. Eisenberg, E. J. S. Fonseca, and D. Bouwmeester, Phys. Rev. Lett. **96**, 203601 (2006).
[19] R. Okamoto, H. F. Hofmann, T. Nagata, J. L. O'Brien, K. Sasaki, and S. Takeuchi, New J. Phys. **10**, 073033 (2008).
[20] C. C. Gerry, Phys. Rev. A **61**, 043811 (2000).
[21] C. C. Gerry and R. A. Campos, Phys. Rev. A **64**, 063814 (2001).
[22] A. Datta, L. Zhang, N. Thomas-Peter, U. Dorner, B. J. Smith, and I. A. Walmsley, Phys. Rev. A **83**, 063836 (2011).
[23] I. Afek, O. Ambar, and Y. Silberberg, Phys. Rev. Lett. **104**, 123602 (2010).
[24] D. Schuster, A. Houck, J. Schreier, A. Wallraff, J. Gambetta, A. Blais, L. Frunzio, J. Majer, B. Johnson, M. Devoret *et al.*, Nature (London) **445**, 515 (2007).
[25] D. Achilles, C. Silberhorn, C. Sliwa, K. Banaszek, I. A. Walmsley, M. J. Fitch, B. C. Jacobs, T. B. Pittman, and J. D. Franson, J. Mod. Opt. **51**, 1499 (2004).
[26] D. Achilles, C. Silberhorn, C. Śliwa, K. Banaszek, and I. A. Walmsley, Opt. Lett. **28**, 2387 (2003).
[27] A. Peres, *Quantum Theory: Concepts and Methods* (Springer Science & Business Media, 2006), Vol. 57.
[28] J. Lundeen, A. Feito, H. Coldenstrodt-Ronge, K. Pregnell, C. Silberhorn, T. Ralph, J. Eisert, M. Plenio, and I. Walmsley, Nat. Phys. **5**, 27 (2009).
[29] M. G. Genoni, S. Olivares, and M. G. A. Paris, Phys. Rev. Lett. **106**, 153603 (2011).
[30] U. Dorner, R. Demkowicz-Dobrzanski, B. J. Smith, J. S. Lundeen, W. Wasilewski, K. Banaszek, and I. A. Walmsley, Phys. Rev. Lett. **102**, 040403 (2009).
[31] K. P. Seshadreesan, P. M. Anisimov, H. Lee, and J. P. Dowling, New J. Phys. **13**, 083026 (2011).
[32] L. Pezzé and A. Smerzi, Phys. Rev. Lett. **100**, 073601 (2008).